LiDAR-based map of an active, normal fault: Teton fault, Wyoming

Hanson, Jared J., Colwell, Christopher L., Willis, Dr. Julie B.

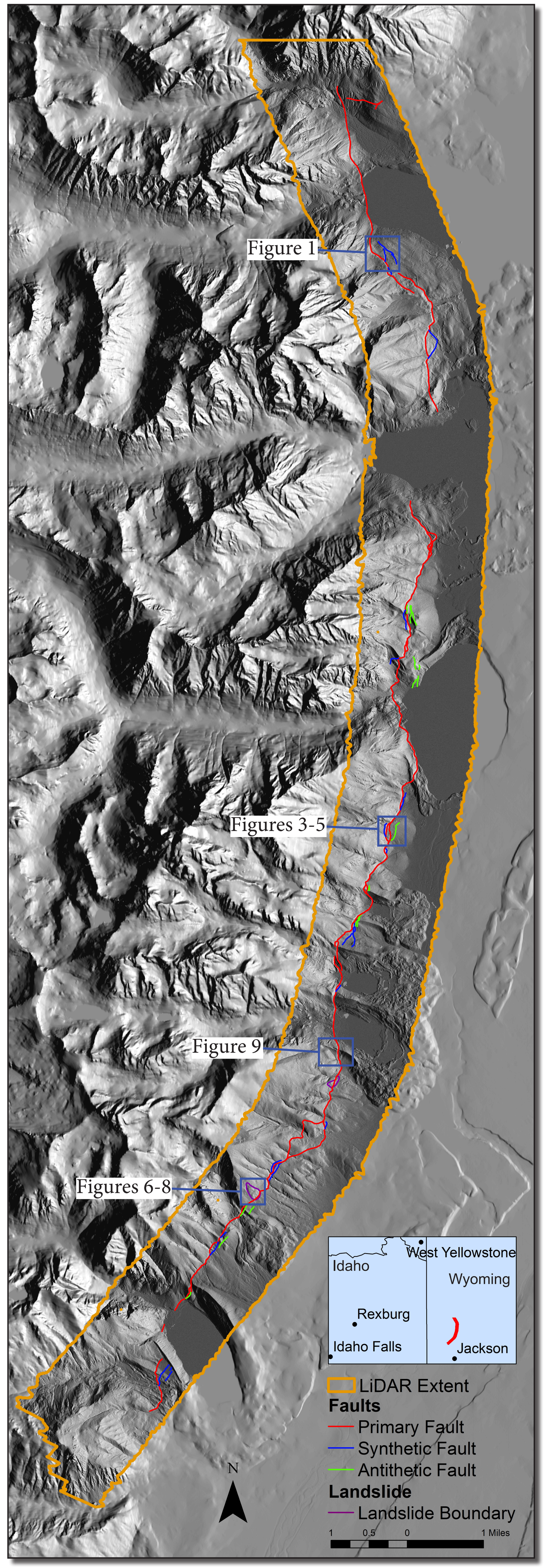

Abstract

Bare earth LiDAR data (<1 m resolution) are used to create a new map of the Teton fault, an active normal fault in western Wyoming. Several differences exist between our LiDAR-based map and previously published maps of the Teton fault (Fig. 1).

LiDAR data provide high resolution topographic models of earth's surface as if it were stripped of vegetation and is used to analyze subtle changes in surface topography. Bare earth data are particularly useful for mapping fault scarps and subtle synthetic and antithetic splays that are typically obscured by vegetation or otherwise unrecognized (Fig. 1). To elicit the primary and secondary scarps of the Teton fault, we applied four different GIS analyses (hillshade, slope, aspect and contour) and adjusted colors, stretch and lighting to further enhance the fault-related lineations. Each analysis provides a unique way to view the scarps, and together they strengthen our interpretations. The primary fault is expressed as a large north-south striking, eastward dipping linear feature on the eastern edge of the Teton Range; offset on the scarp varies along strike, but can be as great as 30 m. The scarps of synthetic splays are small linear features with similar strike and dip to the primary fault; antithetic splays are small, similar-striking, opposite-dipping lineations (Fig. 2).

Our analysis of the LiDAR data also revealed several previously unmapped landslides, many of which obscure the primary fault scarp and resulted in some of the fault discontinuities found on previous maps. Further research will be conducted this summer to field verify the existence of the fault splays and to analyze some of the more complicated areas.

Accurately mapping normal faults and their splays provides better measures of the amount of total fault slip and the continuous length of the fault as well as the location of the areas of highest slip, overlaps, and stepovers. These data are used to develop accurate hazard analysis models. The data gathered also provide details on the interaction between the primary fault and earth's surface, which may lead to a better understanding of near-surface fault mechanics and the formation of antithetic and synthetic splays.

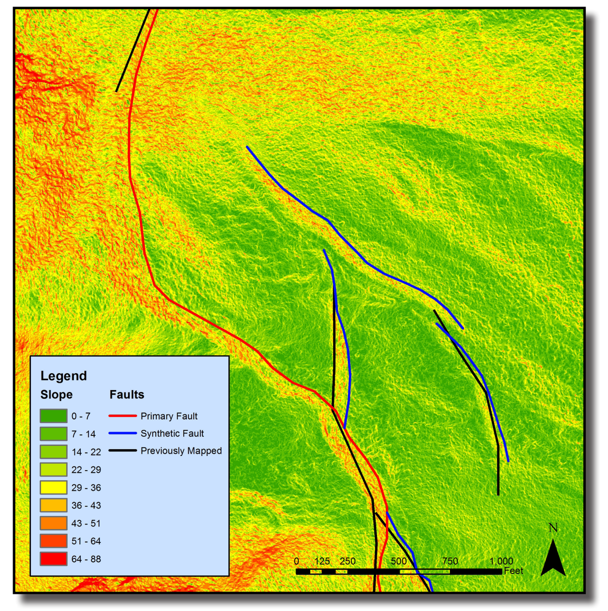

Figure 1. Previously Mapped Faults. High resolution LiDAR provides a more detailed map of the Teton fault. Previously unseen scarps become visible and more accurate fault lines can be mapped. (Slope measured in degrees from horizontal.)

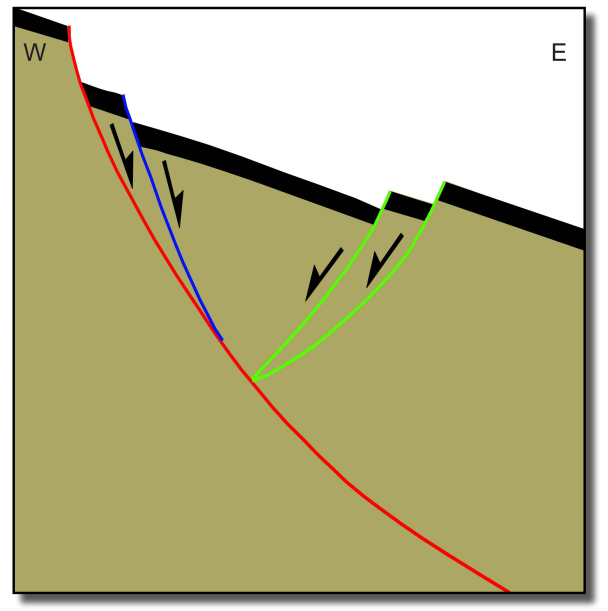

Figure 2. Idealized cross-section of the Teton fault. The Teton fault is a north-south striking, eastward-dipping listric normal fault (red line). Smaller faults that are similar in strike and dip are synthetic splays (blue line). Smaller faults that are similar in strike but opposite in dip to the main fault are antithetic splays (green lines).

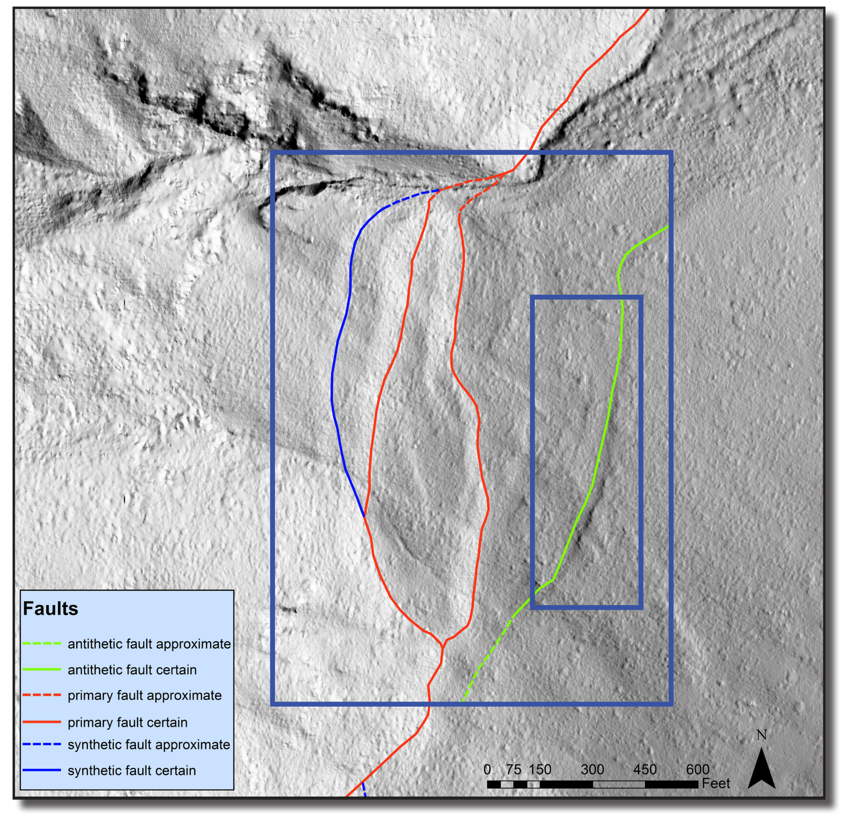

Figure 3. Hillshade. The hillshade analysis allows for artificial illumination of the ground surface. Low sun angles at an azimuth perpendicular to the fault scarp work best. (az. = 90°, alt. = 30°)

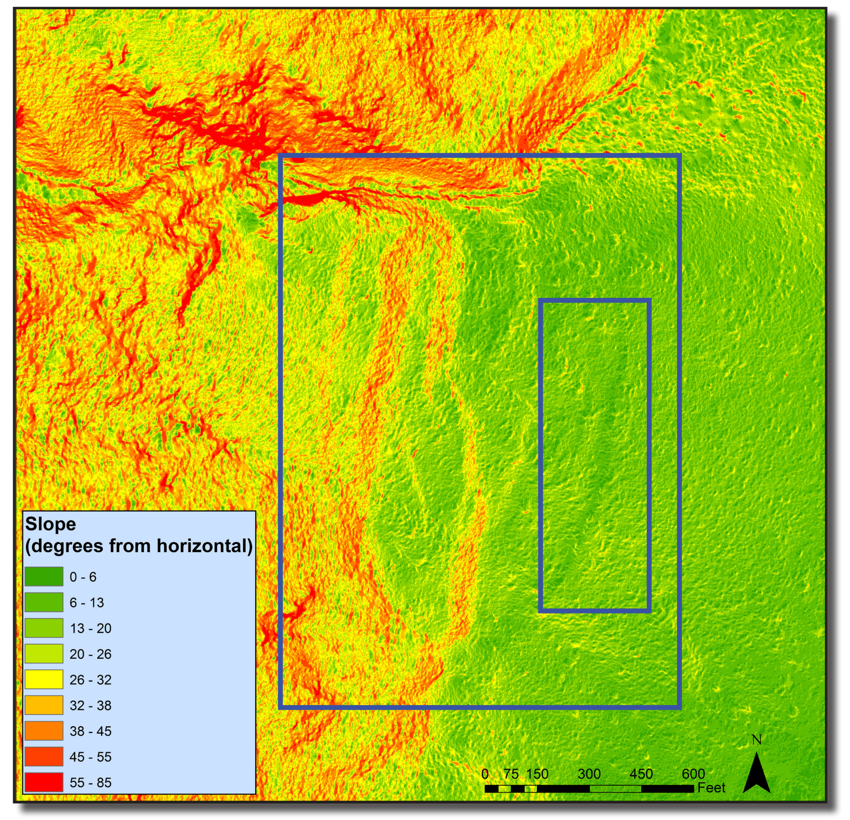

Figure 4. Slope. The slope analysis depicts the steepness of the slope. The fault scarp is shown by red lineations. In this section, multiple bands of red indicate fault splays.

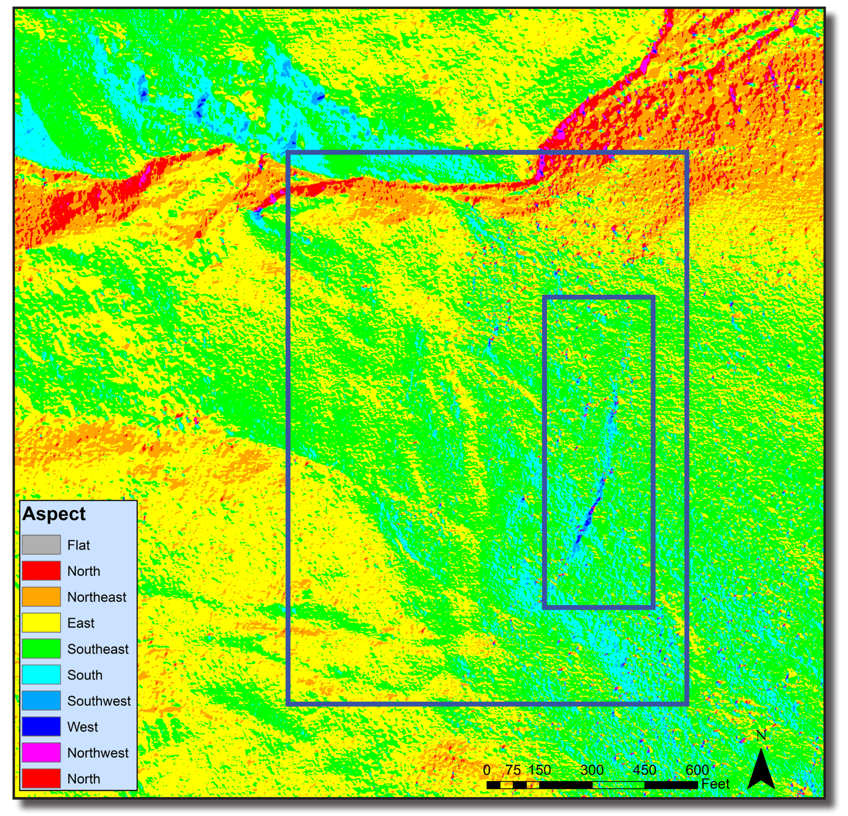

Figure 5. Aspect. The aspect analysis shows the direction of slope. The blue lineation indicated by the small box is interpreted as the fault scarp of an antithetic splay (Fig. 1).

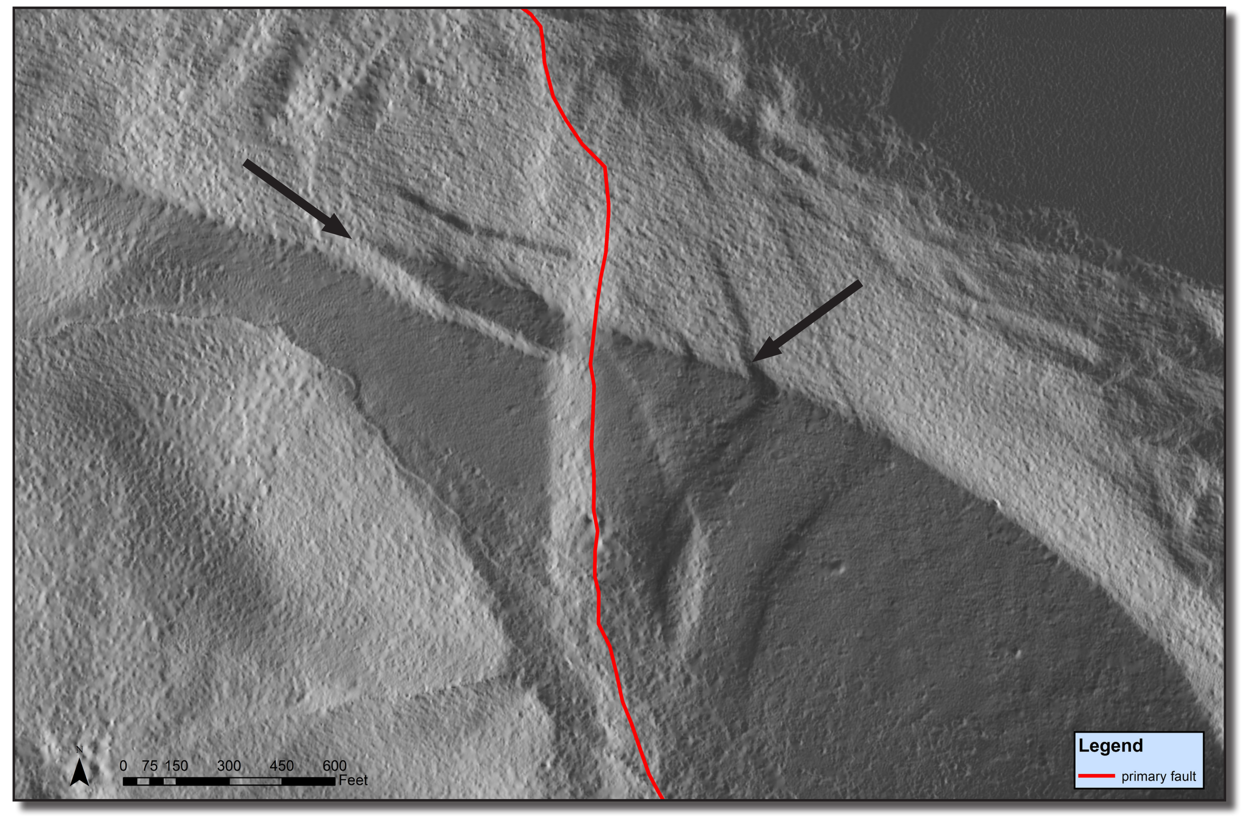

Figure 9. Place of Interest. This image shows a complex section of the fault on a lateral moraine. A transparent hillshade (az. = 90°, alt. = 30°) overlays a stretched slope analysis. Arrows indicate features that may represent faults. We have yet to come to a concensus on the fault locations and types.

Methods

Linear features with sharp relief are key indicators of a fault scarp. The primary Teton fault is the simplest to find as it is a large north-south striking, eastward dipping linear feature. Synthetic splays are identified by smaller scarps with similar strike and dip to the primary fault. Antithetic splays are identified by smaller similar-striking, opposite-dipping scarps. Four GIS analyses were run on the LiDAR data: hillshade, slope, aspect, and contour (Fig. 3-5, 7). These four analyses provide unique ways of finding and interpreting the fault. Hillshades with an azimuth perpendicular to the fault combined with low sun angles give the best results. These created either linear shadows or bright spots on the fault scarp (Fig. 3). The slope analysis displays higher gradients as red and lower gradients as green. This is useful because the fault scarp generally has a steeper slope than the ground around it and appears as a bright red band (Fig. 4). Aspect displays the direction of slope in relation to cardinal (N, S, E, W) and ordinal (NE, NW, SE, SW) directions as different colors. This is not useful in discriminating between the primary fault and synthetic fault as these face the same direction as the rest of the slope, but is very effective in locating antithetic splays (Fig. 5). Contour are used to help identify landslides which obscured the fault scarp (Fig. 6-8).

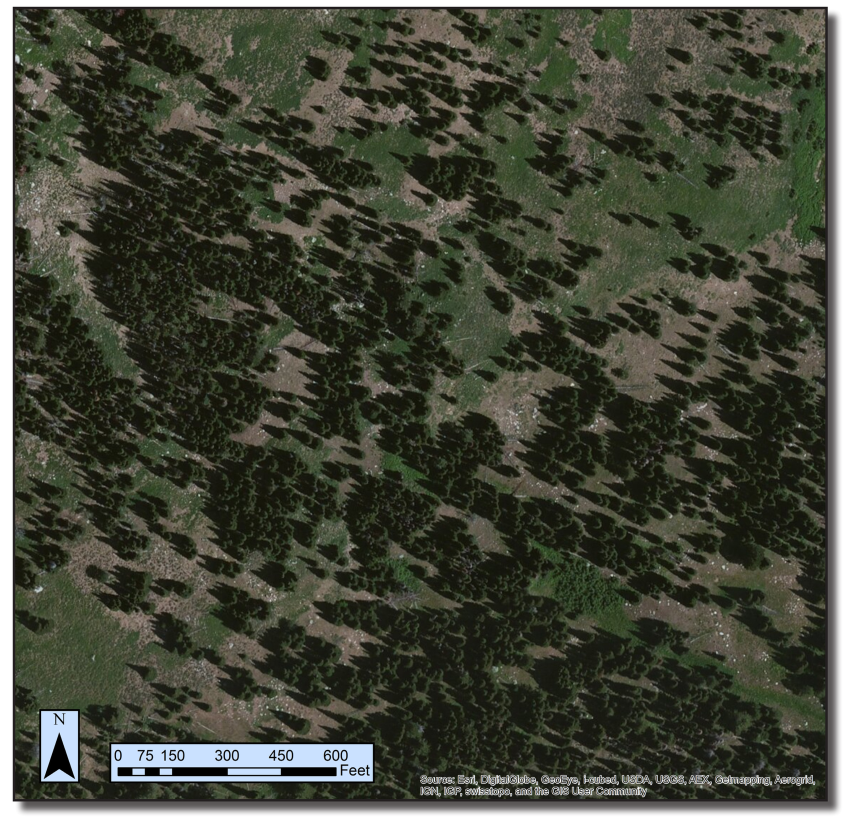

Figure 6. Satellite image of area of interest. LiDAR allows for analysis of the bare earth (Fig. 7-8), effectively "removing" vegetation.

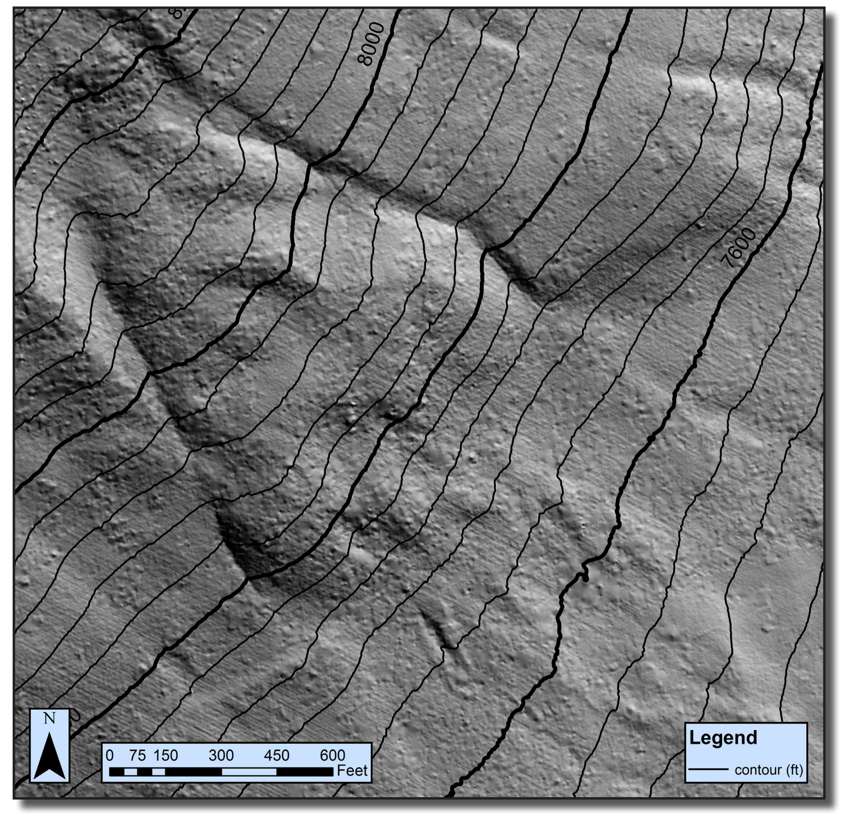

Figure 7. Contour. Contours are convex uphill at the head and convex downhill at the toe of a landslide. (az. = 30°, alt. = 30°, at 30% transparency) (az. = 60°, alt. = 30°)

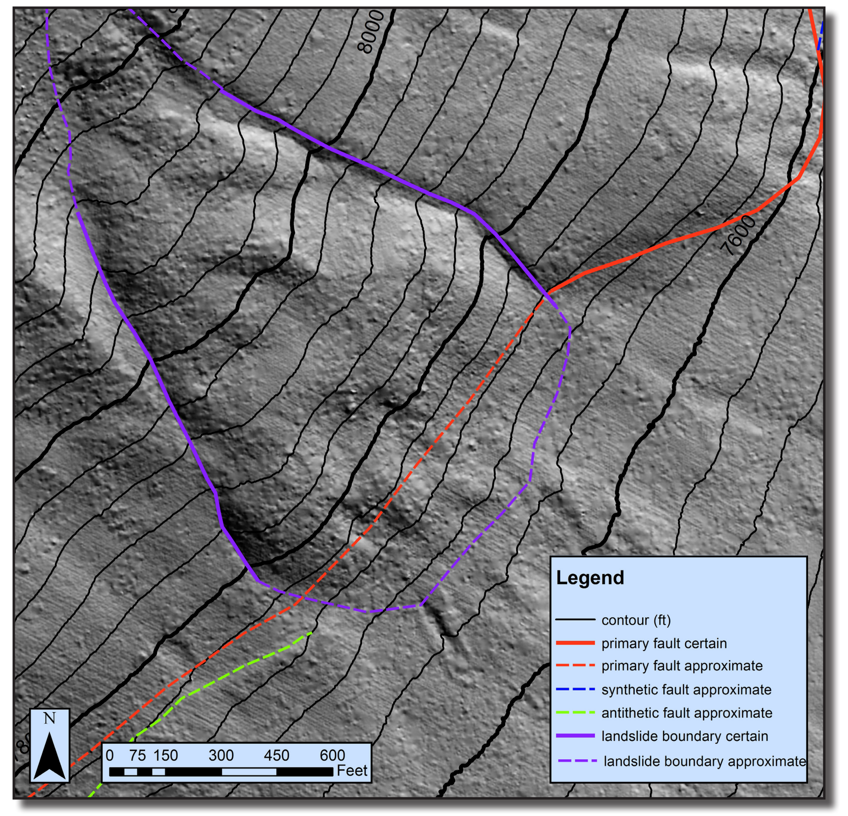

Figure 8. Mapped landslide and faults. A map of the landslide and faults as interpreted from the contours and other analyses. (az. = 30°, alt. = 30°, at 30% transparency) (az. = 60°, alt. = 30°)

Future Research

- Mapped faults and landslides will be field truthed this summer. We will focus on and study in further detail the more complex areas (e.g., Fig. 9).
- This detailed map of an active normal fault zone will allow for more accurate modeling of the interactions between a primary normal fault and its subsidiary faults. Coulomb 3.3 will be used to simulate possible fault ruptures and calculate stress transfer between the primary fault and the antithetic and synthetic splays.
- The models and map will be used to more accurately evaluate earthquake hazards and increase understanding of interactions between fault splays.

Acknowledgements

The data were collected through Earth Scope, a program dedicated to increasing knowledge about the North American continent. This program is funded by the National Science foundation. Dr. Bob Smith at the University of Utah was influential in having the LiDAR flown.

References

Byrd, J.O.D., Smith, R.B., and Geissman, J.W., 1994, The Teton fault, Wyoming: Topographic signature, neotectonics, and mechanisms of deformation: Journal of geophysical research., v. 99, p. 20,095.

Doser, D.I., and Smith, R.B., 1983, Seismicity of the Teton-southern Yellowstone region, Wyoming: Bulletin of the Seismological Society of America, v. 73, p. 1369–1394.

Hampel, A., Hetzel, R., and Densmore, A.L., 2007, Postglacial slip-rate increase on the Teton normal fault, northern Basin and Range Province, caused by melting of the Yellowstone ice cap and deglaciation of the Teton Range?: Geology, v. 35, p. 1107–1110, doi: 10.1130/G24093A.1.

Hampel, A., Hetzel, R., Maniatis, G., and Karow, T., 2009, Three-dimensionzal numerical modeling of slip rate variations on normal and thrust fault arrays during ice cap growth and melting: Journal of Geophysical Research: Solid Earth, v. 114, p. n/a–n/a, doi: 10.1029/2008JB006113.

Leopold, E.B., Liu, G., Love, J.D., and Love, D.W., 2007, Plio-Pleistocene climatic transition and the lifting of the Teton Range, Wyoming: Quaternary Research, v. 67, p. 1–11, doi: 10.1016/j.yqres.2006.10.006.

White, B.J.P., Smith, R.B., Husen, S., Farrell, J.M., and Wong, I., 2009, Seismicity and earthquake hazard analysis of the Teton–Yellowstone region, Wyoming: Journal of Volcanology and Geothermal Research, v. 188, p. 277–296, doi: 10.1016/j.jvolgeores.2009.08.015.